## Research

CrossMark
click for updates

**Author for correspondence:**
Peter J. Gawthrop
e-mail: peter.gawthrop@unimelb.edu.au

# Energy-based analysis of biochemical cycles using bond graphs

Peter J. Gawthrop[1] and Edmund J. Crampin[1,2,3]

[1]Systems Biology Laboratory, Melbourne School of Engineering, University of Melbourne, [2]Department of Mathematics and Statistics, and [3]School of Medicine, University of Melbourne, Victoria 3010, Australia

Thermodynamic aspects of chemical reactions have a long history in the physical chemistry literature. In particular, biochemical cycles require a source of energy to function. However, although fundamental, the role of chemical potential and Gibb's free energy in the analysis of biochemical systems is often overlooked leading to models which are physically impossible. The bond graph approach was developed for modelling engineering systems, where energy generation, storage and transmission are fundamental. The method focuses on how power flows between components and how energy is stored, transmitted or dissipated within components. Based on the early ideas of network thermodynamics, we have applied this approach to biochemical systems to generate models which automatically obey the laws of thermodynamics. We illustrate the method with examples of biochemical cycles. We have found that thermodynamically compliant models of simple biochemical cycles can easily be developed using this approach. In particular, both stoichiometric information and simulation models can be developed directly from the bond graph. Furthermore, model reduction and approximation while retaining structural and thermodynamic properties is facilitated. Because the bond graph approach is also modular and scaleable, we believe that it provides a secure foundation for building thermodynamically compliant models of large biochemical networks.

Royal Society **Publishing**

# 1. Introduction

*Oh ye seekers after perpetual motion, how many vain chimeras have you pursued? Go and take your place with the alchemists.*

<div align="right">Leonardo da Vinci, 1494</div>

Thermodynamic aspects of chemical reactions have a long history in the physical chemistry literature. In particular, the role of chemical potential and Gibb's free energy in the analysis of biochemical systems is developed by, for example, Hill [1], Beard & Qian [2] and Keener & Sneyd [3]. As discussed by, for example, Katchalsky & Curran [4] and Cellier [5, ch. 8], there is a distinction between classical thermodynamics which treats closed systems which are in equilibrium or undergoing reversible processes and non-equilibrium thermodynamics which treats systems, such as living organisms, which are open and irreversible.

Biochemical cycles are the building-blocks of biochemical systems; as discussed by Hill [1], they require a source of energy to function. For this reason, the modelling of biochemical cycles requires close attention to thermodynamical principles to avoid models which are physically impossible. Such physically impossible models are analogous to the perpetual motion machines beloved of inventors. In the context of biochemistry, irreversible reactions are *not*, in general, thermodynamically feasible and can be erroneously used to move chemical species against a chemical gradient thus generating energy from nothing [6]. The theme of this paper is that models of biochemical networks must obey the laws of thermodynamics; therefore, it is highly desirable to specify a modelling framework in which compliance with thermodynamic principles is automatically satisfied. Bond graphs provide one such framework.

Bond graphs were introduced by Henry Paynter (see [7] for a history) as a method of representing and understanding complex multi-domain engineering systems such as hydroelectric power generation. A comprehensive account of bond graphs is given by Gawthrop & Smith [8], Borutzky [9] and Karnopp *et al.* [10] and a tutorial introduction for control engineers is given by Gawthrop & Bevan [11].

As discussed by, for example, Palsson [12,13], Alon [14] and Klipp *et al.* [15], the numerous biochemical reactions occurring in cellular systems can be comprehended by arranging them into *networks* and analysing them by graph theory and using the associated connection matrices. These two aspects of biochemical reactions—thermodynamics and networks—were brought together some time ago by Oster *et al.* [16]. A comprehensive account of the resulting *network thermodynamics* is given by Oster *et al.* [17]. As discussed by Oster & Perelson [18] such thermodynamic networks can be analysed using an equivalent electrical circuit representation; but, more generally, the bond graph approach provides a natural representation for network thermodynamics [17,19,20]. This approach was not widely adopted by the biological and biochemical modelling community and may be considered to have been ahead of its time. Mathematical modelling and computational analysis of biochemical systems have developed a great deal since then, and now underpins the new disciplines of systems biology [21], and 'physiome' modelling of physiological systems [22–25], where we are faced with the need for physically feasible models across spatial and temporal scales of biological organization.

In particular, there has been a resurgence of interest in this approach to modelling as it imposes extra constraints on models, reducing the space of possible model structures or solutions for consideration. This has been applied from individual enzymes [26,27] and cellular pathways [28] up to large-scale models [29–31], as a way of eliminating thermodynamically infeasible models of biochemical processes and energetically impossible solutions from large-scale biochemical network models alike (see [32] for a review). Additionally, there is new impetus into model sharing and reuse in the biochemical and physiome modelling communities which has garnered interest in modular representations of biochemical networks and has promoted development of software, languages and standards and databases for models of biochemical processes. Model representation languages such as CellML and SBML promote model sharing through databases such as the Physiome Model Repository and BioModels Database. Descriptions of models in a hierarchical and modular format allows components of models to be stored in such databases

and assembled into new models. Rather than revisiting the detailed theoretical development, therefore, our aim is to refocus attention on the bond graph representation of biochemical networks for practical purposes such as these. First we briefly review the utility of the bond graph approach with these aims in mind.

Bond graph approaches have also developed considerably in recent years, in particular, through the development of computational tools for their analysis, graphical construction and manipulation, and modularity and reuse [33–38], which are key preoccupations for systems biology and physiome modelling. Our focus is on how kinetics and thermodynamic properties of biochemical reactions can be represented in this framework, and how the bond graph formalism allows key properties to be calculated from this representation. In addition, bond graph approaches have been extended in recent years to model electrochemical storage devices [39] and heat transfer in the context of chemical reactions [40]. Cellier [5] extends network thermodynamics beyond the isothermal, isobaric context of Oster *et al.* [17] by accounting for both work and heat, and a series of papers [37,41] shows how multi-bonds can be used to model the thermodynamics of chemical systems with heat and work transfer and convection and to simulate large systems. Thoma & Atlan [42] discuss 'osmosis as chemical reaction through a membrane'. LeFèvre *et al.* [43] model cardiac muscle using the bond graph approach.

Bond graphs explicitly model the flow of energy through networks making use of the concept of power covariables: pairs of variable whose product is power. For example, in the case of electrical networks, the covariables are chosen as voltage and current. As discussed in earlier studies [1,5,44,45], chemical potential is the driving force of chemical reactions. Hence, as discussed by Cellier [5], the appropriate choice of power covariables for isothermal, isobaric chemical reaction networks is chemical potential and molar flow rates. As pointed out by Beard *et al.* [30], using both mass and energy balance ensures that models of biochemical networks are thermodynamically feasible. Modelling using bond graphs automatically ensures not only mass balance but also energy balance; thus models of biochemical networks developed using bond graphs are thermodynamically feasible.

As discussed by Hill [1], biochemical cycles are the building-blocks of biochemical systems. Bond graph models are able to represent thermodynamic cycles and therefore appropriately represent free energy transduction in biochemical processes in living systems.

Living systems are complex, and therefore a hierarchical and modular approach to modelling biochemical systems is desirable. Bond graphs have a natural hierarchical representation [46] and have been used to model complex network thermodynamics [5,37,41]. Complex systems can be simplified by approximation: the bond graph method has a formal approach to approximation [8,10,11] and the potential algebraic issues arising from such approximation [47]. In particular, complex systems can be simplified if they exhibit a fast and slow timescale; a common feature of many biochemical (for example, Michaelis–Menten enzyme kinetics) and cell physiological systems (for example, slow–fast analysis of the membrane potential of electrically excitable cells). A bond graph approach to two-time-scale approximation has been presented by Sueur & Dauphin-Tanguy [48].

As well as providing a thermodynamically consistent model of a dynamical system suitable for simulation, representation of a biochemical system using the bond graph approach enables a wide range of properties and characteristics of the system to be represented. A number of key physical properties can be derived directly from the bond graph representation. For example, chemical reactions involve interactions between species which preserve matter; the number of moles of each species in a reaction must be accounted for.

As discussed by Oster *et al.* [17, §5.2], the kinetics of biochemical networks become particularly simple near thermodynamic equilibrium. However, as discussed by Qian & Beard [49], it is important to consider the behaviour of biochemical networks in living systems far from equilibrium. In particular, the analysis of non-equilibrium steady states (where flows are constant but non-zero and states are constant) is important [2,50].

Using elementary reactions as examples, §2 shows how biochemical networks may be modelled using bond graphs. The bond graph is more than a sketch of a biochemical network; it
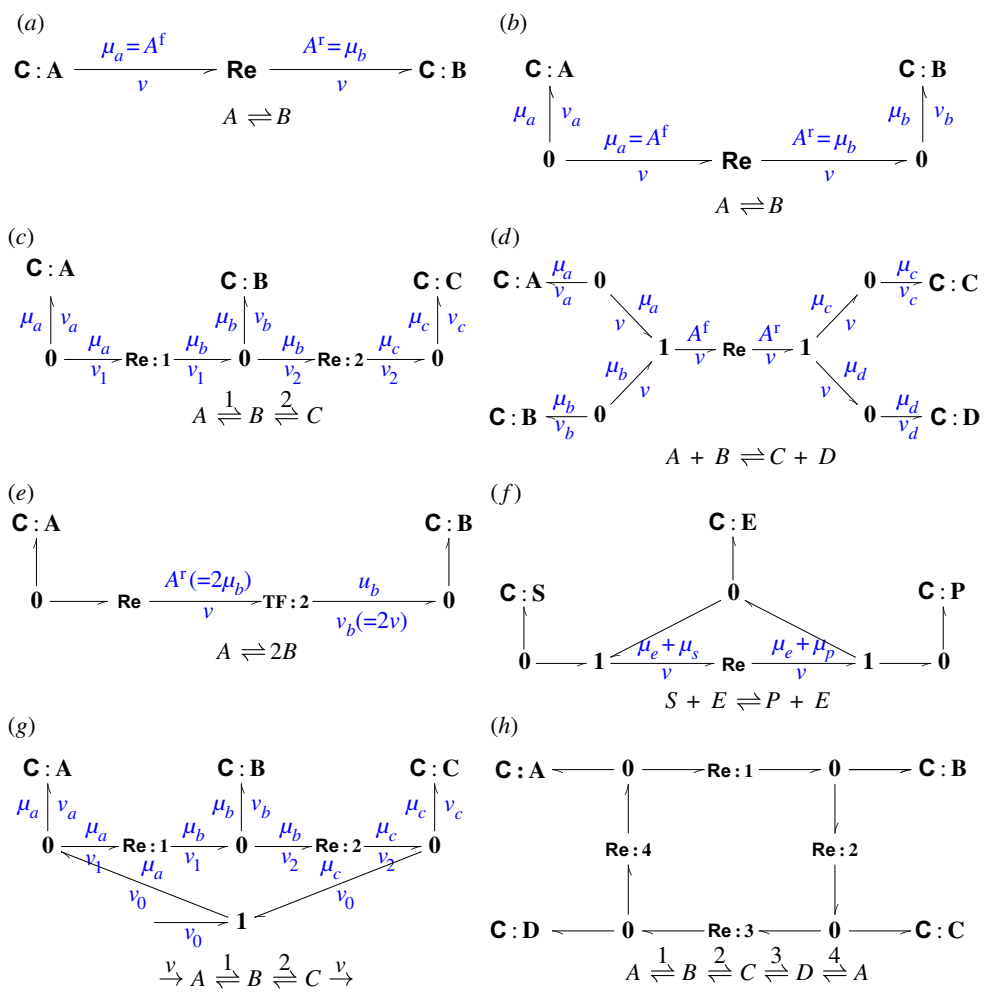
**Figure 1.** Simple reactions and their bond graphs. (*a*) The simple binary reaction is represented by a bond graph using a **C** component for each substance and an **Re** component to explicitly represent the reaction. (*b*) An alternative representation using **0** (common potential) junctions to allow connections. (*c*) Two reactions in series extending (*b*). (*d*) A single reaction between four substances requires a single **Re** component, one **C** component for each substance and two **1** (common flow) connections. (*e*) The stoichiometric coefficient 2 can be incorporated using the bond graph **TF** component. (*f*) A simple enzyme-catalysed reaction. The enzyme *E* appears on each side of the formula thus creating a cycle in the bond graph (see §5*a*). (*g*) The same as (*c*) but with an externally imposed flow that adds molecules of *A* while subtracting the same number of molecules of *C* thus allowing a non-equilibrium steady state. (*h*) A simple biochemical cycle. (Online version in colour.)

can be directly interpreted by a computer and, moreover, has a number of features that enable key physical properties to be derived from the bond graph itself. For example, §3 shows how the bond graph can be used to examine the *stoichiometric* properties of biochemical networks. Section 4 discusses the role of bond graphs in the structural approximation of biochemical networks. Section 5 discusses two biochemical cycles, an enzyme catalysed reaction and a biochemical switch, to illustrate the main points of the paper. Section 6 discusses software aspects of the bond graph approach and how it could be integrated into preexisting hierarchical modelling frameworks. Section 7 concludes the paper.

## 2. Bond graph modelling of chemical reactions

Bond graphs are an energy-based modelling approach. This section introduces the bond graph methodology in the context of biochemical reactions using the reactions listed in figure 1. The

section is organized to emphasize the key aspects of bond graph modelling which make it a powerful approach to the modelling of biochemical systems.

## (a) Energy flow, storage and dissipation in a simple reversible reaction

Figure 1a shows the simple interconversion of two molecular species, A and B. As mentioned above, a thermodynamically consistent representation of biochemical processes demands consideration of reversible reactions, and so we consider this simple interconversion as the simplest possible reaction. This interconversion is represented by *bonds* of the form $\frac{\mu}{v}$ each of which is associated with two variables:[1] the *chemical potential* $\mu$ (J mol$^{-1}$) and a *molar flow rate* $v$ (mol s$^{-1}$).[2] The product of these two variables is energy flow or *power* $P = \mu \times v$ (W). The bonds represent the transmission of power in the system and do not create, store or dissipate power. The half-arrow on the bond indicates the direction in which power flow will be regarded as positive and thus defines a sign convention.

In figure 1a, the pools of chemical species A and B are represented by **C** components. These components reflect the amount of each species present (and hence determine the chemical potential of each species).[3] **C**: **A** contains $x_a$ moles of species $A$ and the rate of decrease is equal to the molar flow $v$; **C**: **B** contains $x_b$ moles of species $B$ and the rate of increase is $v$. Thus

$$\dot{x}_a = -v \quad \text{and} \quad \dot{x}_b = v. \tag{2.1}$$

Each **C** component is associated with a chemical potential $\mu$ which, assuming a dilute system within a volume $V$, is given by Keener & Sneyd [3, §1.2]:

$$\mu_a = \mu_a^0 + RT \ln \frac{x_a}{V} \quad \mu_b = \mu_b^0 + RT \ln \frac{x_b}{V}, \tag{2.2}$$

where $\mu_a^0$ is the standard chemical potential for species A, and similarly for species B. It is convenient to rewrite equations (2.2) as

$$\mu_a = RT \ln K_a x_a, \quad \mu_b = RT \ln K_b x_b, \quad \text{where } K_a = \frac{1}{V} e^{\mu_a^0/RT} \quad \text{and} \quad K_b = \frac{1}{V} e^{\mu_b^0/RT}. \tag{2.3}$$

Each **C** component *stores* but does not create or dissipate energy. The corresponding energy flow is described through the bond to which it is connected.

The reversible reaction between chemical species $A$ and $B$ is represented by a single **Re** (Reaction) component which relates the reaction flow $v$ to the chemical affinities (weighted sum of chemical potentials) for the forward and reverse reactions $A^f = \mu_a$ and $A^r = \mu_b$. As discussed by Van Rysselberghe [51] and Oster *et al.* [17, §5.1], the reaction rate, or molar flow, is given by the *Marcelin–de Donder* formula:

$$v = v^+ - v^-, \quad \text{where } v^+ = \kappa \, e^{A^f/RT} \quad \text{and} \quad v^- = \kappa \, e^{A^r/RT}, \tag{2.4}$$

where $\kappa$ is a constant which determines reaction rate. This can be rewritten in two ways. The *de Donder* formula [52, eqn(11)]:

$$\frac{v^+}{v^-} = e^{A/RT}, \quad \text{where } A = A^f - A^r \tag{2.5}$$

and the *Marcelin* formula [53, eqn(1)]:

$$v = \kappa (e^{A^f/RT} - e^{A^r/RT}). \tag{2.6}$$

---

[1]The textual annotation in blue is for explanatory purposes, it is not part of the bond graph itself.

[2]The standard bond graph terminology is that the chemical potential is termed an *effort* and is analogous to voltage in electrical systems and force in mechanical systems. Similarly, the molar flow rate is termed a *flow* and analogous to current in electrical systems and velocity in mechanical systems.

[3]The **C** component stands for 'capacitor'. The chemical potential is analogous to the voltage associated with a capacitor in an electrical circuit, which charges or discharges if there is a net influx or efflux into the component.

**6**

rspa.royalsocietypublishing.org  *Proc. R. Soc. A* **470**: 20140459

This latter formulation is used in the sequel. The **Re** component *dissipates* but does not create or store, energy.

In the particular case of figure 1*a*, substituting the chemical potentials of equations (2.3) into equations (2.4) recovers the well-known first-order mass-action expressions:

$$v^+ = \kappa K_a x_a \quad \text{and} \quad v^- = \kappa K_b x_b, \quad v = \kappa(K_a x_a - K_b x_b). \tag{2.7}$$

We note that this notation clearly demarcates parameters relating to thermodynamic quantities $(K_a, K_b)$ from reaction kinetics $(\kappa)$ and that the equilibrium constant is given by $K_b/K_a$.

Equations (2.7) can also be written in the conventional rate constant form as

$$v^+ = k^+ x_a \quad \text{and} \quad v^- = k^- x_b, \quad v = v^+ - v^- = k^+ x_a - k^- x_b, \tag{2.8}$$

where the forwards and backwards first-order rate constants are

$$k^+ = \kappa K_a \quad \text{and} \quad k^- = \kappa K_b. \tag{2.9}$$

The thermodynamic quantities and reaction kinetics are no longer distinguished in the rate constant formulation of equations (2.8).

## (b) Modularity: coupling reactions into networks

A key feature of bond graph representations is to construct and analyse models of large-scale systems from simpler building blocks. The bond graph of figure 1*a* cannot be used as a building block of a larger system as there are no connections available with which to couple to other reactions. However, the bond graph approach is, in general, modular and provides two connection components for this purpose: the **0** junction and the **1** junction. Each of these components transmits but does not store, create or dissipate energy. In figure 1*b*, the representation of the simple reversible reaction in figure 1*a* is expanded to include two **0** junction connectors. This representation is identical to that in figure 1*a* except that it makes explicit the junctions through which other reactions involving species A and B can be coupled to this reaction. The bond graph of figure 1*c* makes use of the right-hand **0** junction of figure 1*b* to build two connected reactions; where species B is also reversibly interconverts with species C.

The connector in this case is a **0** junction. The **0** junction can have two or more impinging bonds. In the case of the central **0** junction of figure 1*c*, there are three impinging bonds: one $\left(\genfrac{}{}{0pt}{}{\mu_b}{\xrightarrow{\phantom{x}}\, v_1}\right)$ pointing in and two $\left(\genfrac{}{}{0pt}{}{\mu_b}{\xrightarrow{\phantom{x}}\, v_b} \text{ and } \genfrac{}{}{0pt}{}{\mu_b}{\xrightarrow{\phantom{x}}\, v_2}\right)$ pointing out. As indicated in figure 1*c*, the **0** junction has two properties:

(i) the chemical potentials or affinities (*efforts*) on all impinging bonds are constrained to be the same, (the **0** junction is therefore a *common potential* connector) and
(ii) the molar *flows* on the impinging bonds sum to zero, under the sign convention that a plus sign is appended to the flows corresponding to inward bonds and a minus sign for outward bonds:

$$v_1 - v_b - v_2 = 0 \quad \text{or} \quad v_b = v_1 - v_2. \tag{2.10}$$

These two properties imply a third: the power flowing out of a **0** junction is equal to the power flowing in (the **0** junction is power-conserving):

$$P_a + P_2 = \mu_b v_b + \mu_b v_2 = \mu_b(v_b + v_2) = \mu_b v_1 = P_1. \tag{2.11}$$

In a similar manner, the left-hand **0** junction implies that $v_a = -v_1$ and the right-hand **0** junction implies that $v_c = v_2$. Figure 1*c* can easily be extended to give a reaction chain of arbitrary length.

By contrast, in order to represent the reaction of figure 1*d* we introduce the **1** junction, which has the same power-conserving property as the **0** junction but which represents a *common flow* connector.[4] In particular, with reference to the left-hand **1** junction in figure 1*d*:

(i) the *molar flows* on all impinging bonds are constrained to be the same and
(ii) the *affinities* on the impinging bonds sum to zero when a plus sign is appended to the efforts corresponding to inward bonds and a minus sign for outward bonds:

$$\mu_a + \mu_b - A^{\mathrm{f}} = 0 \quad \text{or} \quad A^{\mathrm{f}} = \mu_a + \mu_b. \tag{2.12}$$

Similarly, the right-hand **1** junction implies that:

$$A^{\mathrm{r}} - \mu_c - \mu_d = 0 \quad \text{or} \quad A^{\mathrm{r}} = \mu_c + \mu_d \tag{2.13}$$

substituting the chemical potentials of equations (2.12) and (2.13) into equations (2.4) gives the well-known second-order mass-action expression:

$$v = \kappa(K_a x_a K_b x_b - K_c x_c K_d x_e) = k^+ x_a x_b - k^- x_c x_d, \tag{2.14}$$

where

$$k^+ = \kappa K_a K_b \quad \text{and} \quad k^- = \kappa K_c K_d. \tag{2.15}$$

Once again, we note that this notation clearly demarcates parameters relating to thermodynamic quantities $(K_a, K_b, K_c, K_d)$ from reaction kinetics $(\kappa)$.

## (c) Incorporating stoichiometry into reactions

The reaction of figure 1*e* has one mole of species *A* reacting to form two moles of species *B*. The corresponding bond graph uses the **TF**[5] component to represent this stoichiometry. The **TF** component transmits but does not store, create or dissipate energy. Hence, the power out equals the power in. Thus. in the context of figure 1*e*:

$$A^{\mathrm{r}} v = \mu_b v_b \tag{2.16}$$

(noting that in this case $A^{\mathrm{r}}$ is the 'unknown' as $\mu_b$ is determined by the **0** junction).

A **TF** component with ratio $n$ is donated by **TF** : $n$ and is defined by the power conserving property and that the output flow is $n$ times the input flow. As power is conserved, it follows therefore that the input effort is $n$ times the output effort. In the context of figure 1*e*

$$A^{\mathrm{r}} = 2\mu_b \quad \text{and} \quad v_b = 2v. \tag{2.17}$$

Noting that $A_{\mathrm{f}} = \mu_a$ it follows from equations (2.4) that:

$$v = \kappa(K_a x_a - (K_b x_b)^2) = k^+ x_a - k^- x_b^2, \quad \text{where} \quad k^+ = \kappa K_a \quad \text{and} \quad k^- = \kappa K_b^2. \tag{2.18}$$

## (d) Non-equilibrium steady states: reactions with external flows

As has been discussed by many authors, in cells biochemical reactions are maintained away from thermodynamic equilibrium through continual mass and energy flow through the reaction. The reaction of figure 1*g* corresponds to the reaction in figure 1*c* except that an external flow $v_0 > 0$ has been included. This corresponds to adding molecules of *A* and removing molecules of *C* at the same fixed rate. As discussed by Qian *et al.* [50], the reaction has a non-equilibrium steady-state (NESS) corresponding to $v_1 = v_2 = v_0$. This is a steady state because the flows $v_a = v_b = v_c = 0$ and hence $\dot{x}_a = \dot{x}_b = \dot{x}_c = 0$; it is not a thermodynamic equilibrium because $v_1 \neq 0$ and $v_2 \neq 0$.

[4]The common flow **1** junction is the *dual* component of the common effort **0** junction.

[5]Oster *et al.* [17] use the symbol **TD** in place of **TF**.

## (e) Thermodynamic compliance

The bond graph approach ensures thermodynamic compliance: the model may not be correct, but it does obey the laws of thermodynamics. To illustrate this point, consider the biochemical cycle of figure 1$h$. As discussed by, for example, Qian *et al.* [50], a fundamental property of such cycles is the thermodynamic constraint that

$$\frac{k_{+1}k_{+2}k_{+3}k_{+4}}{k_{-1}k_{-2}k_{-3}k_{-4}} = 1. \tag{2.19}$$

This property arises from the requirement for detailed balance around the biochemical cycle. However, as is now shown, the thermodynamic constraint of equation (2.19) is automatically satisfied by the bond graph representation of figure 1$h$.

Similar to equation (2.8), the four reaction flows can be written as

$$v_1 = \kappa_1(K_a x_a - K_b x_b), \ldots, v_4 = \kappa_4(K_d x_d - K_a x_a). \tag{2.20}$$

Alternatively, the four reaction flows of equations (2.20) can be rewritten as

$$v_1 = (k_{+1} x_a - k_{-1} x_b), \ldots, v_4 = (k_{+4} x_d - k_{-4} x_a), \tag{2.21}$$

where

$$k_{+1} = \kappa_1 K_a, \ldots, k_{+4} = \kappa_4 K_d, \quad k_{-1} = \kappa_1 K_b, \ldots, k_{-4} = \kappa_4 K_a. \tag{2.22}$$

Hence

$$\frac{k_{+1}k_{+2}k_{+3}k_{+4}}{k_{-1}k_{-2}k_{-3}k_{-4}} = \frac{\kappa_1 K_a \kappa_2 K_b \kappa_3 K_c \kappa_4 K_d}{\kappa_1 K_b \kappa_2 K_c \kappa_3 K_d \kappa_4 K_a}. \tag{2.23}$$

As each factor of the numerator on the right-hand side of equation (2.23) appears in the denominator, and *vice versa*, then equation (2.19) is satisfied.

# 3. Stoichiometric analysis of reaction networks

Stoichiometric analysis is fundamental to understanding the properties of large networks [12,13, 54]. In particular, computing the left and right null space matrices leads to information about pools and steady-state pathways [55–58]. For example, when analysing reaction networks such as metabolic networks, one may seek to determine for measured rates of change of metabolite concentrations, what are the reaction rates in the network. This question is addressed below. Initially, we will address the inverse problem: for given reaction velocities, what are the rates of change of concentrations of the chemical species? In bond graph terms, this asks the question: 'given the reaction flows $V$, what are the flows $\dot{X}$ at the **C** components?'. This can be addressed directly from the bond graph using the concept of *causality*.

The bond graph concept of causality [8,10,11] has proved useful for generating simulation code, detecting modelling inconsistencies, solving algebraic loops [47], approximation, inversion [59–61] and analysis of system properties [62]. This section shows how the bond graph concept of causality can be used to examine the stoichiometry of networks of biochemical reactions. As in §2, this is done by analysis of particular examples. However, as discussed in §6, this approach scales up to arbitrarily large systems.

## (a) The stoichiometric matrix

Figure 2$a$ is similar to the bond graph of figure 1$a$ except that two lines have been added perpendicular to each bond; these lines are called *causal strokes*. It is convenient to distinguish between the flows on each side of the **Re** component by relabelling them as $v^f$ and $v^r$ ($v^f = v_r = v$) and this is reflected in the annotation. The implications of the causal stroke are twofold:

    (i) the bond imposes *effort* on the component at the stroke end of the bond and
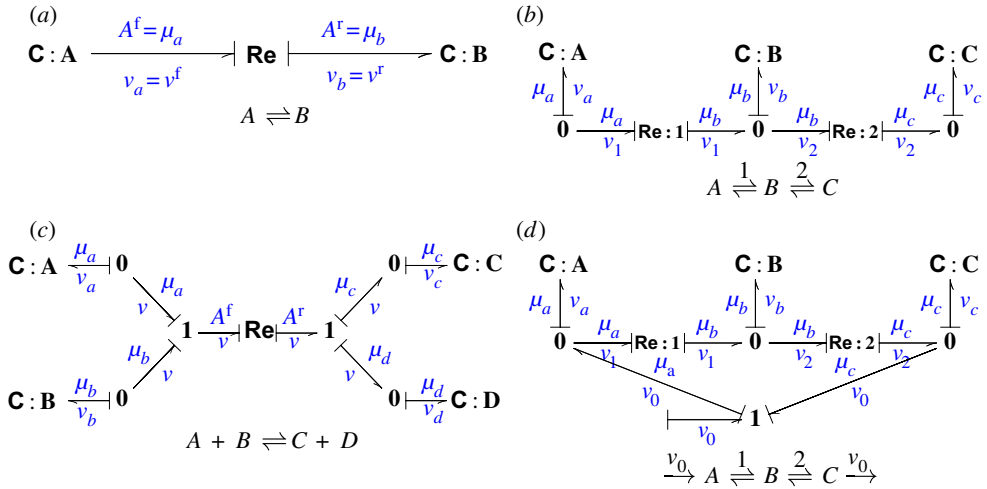    (ii) the bond imposes *flow* on the component at the other end of the bond.

**Figure 2.** Causal strokes and the stoichiometric matrix. The bond graph notion of causality provides an algorithm for determining the stoichiometric matrix by explicitly showing how the **Re** flows propagate to the **C** flows. (*a*) The **C** components impose a potential onto the **Re** component; the **Re** component imposes a flow into the **C** components. (*b*) As (*a*) and note that exactly one bond imposes a potential on to each **0** (common potential) junction. (*c*) As (*a*) and note that exactly one bond imposes a flow on to each **1** (common flow) junction. (*d*) As the external flow $v_0$ impinges on to **0** junctions, it does not affect the causality of the parts in common with (*b*). (Online version in colour.)

Thus, as indicated on the bond graph:[6] the *flows* are given by

$$\dot{x}_a = -v_a = -v^f = -v \quad \text{and} \quad \dot{x}_b = v_b = v^r = v \tag{3.1}$$

and the *efforts* by

$$A_f = \mu_a \quad \text{and} \quad A_r = \mu_b. \tag{3.2}$$

In general, the reaction flows can be composed into the vector $V$, and the state derivatives into the vector $X$ and these are related by the *stoichiometric matrix* $N$:

$$\dot{X} = NV. \tag{3.3}$$

In the case of figure 2*a*:

$$X = \begin{pmatrix} x_a \\ x_b \end{pmatrix} \quad V = v \quad \text{and} \quad N = \begin{pmatrix} -1 \\ 1 \end{pmatrix}. \tag{3.4}$$

The system of figure 2*b* has three **C** components and the state $X$ can be chosen as

$$X = (x_a \quad x_b \quad x_c)^{\mathrm{T}}. \tag{3.5}$$

There are two reaction flows $v_1$ and $v_2$ corresponding to **Re : 1** and **Re : 2**, respectively. The flow vector $V$ can be chosen as

$$V = (v_1 \quad v_2)^{\mathrm{T}}. \tag{3.6}$$

Following the causal strokes and observing the sign convention at the **0** junction

$$\dot{x}_a = v_a = -v_1, \quad \dot{x}_b = v_b = v_1 - v_2 \quad \text{and} \quad \dot{x}_c = v_c = v_2. \tag{3.7}$$

Using (3.5) and (3.6), it follows that

$$\dot{X} = NV, \quad \text{where } N = \begin{pmatrix} -1 & 0 \\ 1 & -1 \\ 0 & 1 \end{pmatrix}.$$

[6] Although in mathematics $x = y$, $y = x$ and $x - y = 0$ are the same, this is not true in imperative programming languages; the left-hand side is computed from the right-hand side. This latter interpretation is used in the rest of this section.
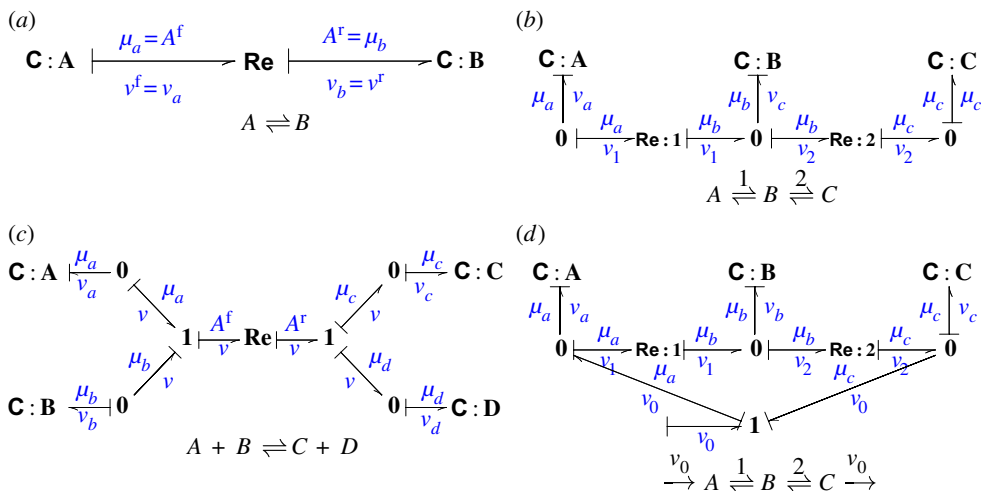
**Figure 3.** Causal strokes and the stoichiometric matrix subspaces. The bond graph notion of causality provides an algorithm for determining the subspaces of the stoichiometric matrix by explicitly showing how the **C** flows propagate to other **C** flows and to the **Re** flows. (*a*) **C** : **A** imposes a flow into **Re** which in turn imposes a flow into **C** : **B**. (*b*) **C** : **A** imposes a flow into **Re** : **1** and thence, together with **C** : **B**. imposes a flow into the **0** junction and thence into **Re** : **2** and **C** : **C**. (*c*) **C** : **A** imposes a flow into the **1** junction and thence into **C** : **B** and **Re**; **Re** in turn imposes a flow into the **1** junction and thence into **C** : **C** and **C** : **D**. (*d*) As the external flow $v_0$ impinges on to **0** junctions, it does not affect the causality of the parts in common with (*b*). (Online version in colour.)

The system of figure 2*d* is similar to that of figure 2*b* but with an additional input $v_0$ and so $V$ is defined as

$$V = (v_0 \quad v_1 \quad v_2)^{\mathrm{T}}. \tag{3.8}$$

Using the summing rules at the left and right **0** junctions, it follows that:

$$\dot{X} = NV, \quad \text{where } N = \begin{pmatrix} 1 & -1 & 0 \\ 0 & 1 & -1 \\ -1 & 0 & 1 \end{pmatrix}.$$

The system of figure 2*c* has 4 **C** components and the state $X$ can be chosen as

$$X = (x_a \quad x_b \quad x_c \quad x_d)^{\mathrm{T}}. \tag{3.9}$$

There is one reaction flows $v$ corresponding to **Re**. The flow vector $V$ is thus scalar in this case:

$$V = v. \tag{3.10}$$

Following the causal strokes and observing the sign convention at the **0** junction,

$$\dot{x}_a = v_a = -v, \quad \dot{x}_b = v_b = -v, \quad \dot{x}_c = v_c = v \quad \text{and} \quad \dot{x}_d = v_d = v. \tag{3.11}$$

Using (3.5) and (3.6), it follows that

$$\dot{X} = NV, \quad \text{where } N = (-1 \quad -1 \quad 1 \quad 1)^{\mathrm{T}}. \tag{3.12}$$

In bond graph terms, this particular arrangement of causal strokes is known as *integral causality*. Naturally, this analysis extends to arbitrarily large systems and can be carried out algorithmically in automated software.

## (b) Stoichiometric null spaces

The causal analysis of §3a asks the question: 'given the reaction flows $V$, what are the flows $\dot{X}$ at the $\mathsf{C}$ components?'. This section looks at the inverse question: 'given the flows $\dot{X}$ at the $\mathsf{C}$ components, what are the reaction flows $V$?'

With this in mind, the causal stroke on the bond impinging on the $\mathsf{C:A}$ component in figure 3a is now at the $\mathsf{C}$ end of the bond, thus imposing flow on the $\mathsf{Re}$ component and so $v^f = v_a$. There is now a causal issue: as $v_r = v_f$, it follows that $v_r$ is also determined by the $\mathsf{C:A}$ component and $v_r = v_a$. Hence the flow on the bond impinging on $\mathsf{C:B}$ is determined and the causality must be as shown. Thus causal considerations show that the flow $v_a$ determines the flow $v_b$ which therefore cannot be independently chosen. In bond graph terms, this particular arrangement of causal strokes is known as *derivative causality*. To summarize,

$$v = v_a = -\dot{x}_a \quad \text{and} \quad \dot{x}_b = v = -\dot{x}_a. \tag{3.13}$$

The system of figure 3a has two $\mathsf{C}$ components and

$$X = (x_a \quad x_b)^{\mathsf{T}}. \tag{3.14}$$

It is convenient to decompose $X$ into two components: $x$ the independent part of $X$ and $X^d$ the dependent part of $X$. In particular,

$$x = x_a = L_{xX}X, \quad \text{where } L_{xX} = (1 \quad 0) \tag{3.15}$$

and

$$X^d = (x_b) = L_{dX}X, \quad \text{where } L_{dX} = (0 \quad 1). \tag{3.16}$$

The full state $X$ can be reconstructed from $x$ and $X^d$ using

$$X = L_{xX}^{\mathsf{T}}x + L_{dX}^{\mathsf{T}}X^d. \tag{3.17}$$

Using this decomposition, equations (3.13) can be written as

$$\dot{X}^d = L_{dx}\dot{x}, \tag{3.18}$$

where

$$L_{dx} = (-1). \tag{3.19}$$

Combining these equations,

$$\dot{X}^d = L_{dX}\dot{X} = L_{dx}\dot{x} = L_{dx}L_{xX}\dot{X}. \tag{3.20}$$

Defining

$$G = L_{dX} - L_{dx}L_{xX} \tag{3.21}$$

it follows that the state dependency can also be expressed as

$$G\dot{X} = GNV = 0, \tag{3.22}$$

where, in this case

$$G = (0 \quad 1) + (1 \quad 0) = (1 \quad 1). \tag{3.23}$$

As discussed in the earlier studies, as (3.22) is true for all $V$

$$GN = 0 \tag{3.24}$$

and thus $G$ is a left null matrix of $N$. In this particular case, $G\dot{X} = 0$ corresponds to

$$\dot{x}_a + \dot{x}_b = 0 \quad \text{or} \quad x_a + x_b = \text{const.} \tag{3.25}$$

Thus, the total amount of $A$ and $B$ is constant.

The system of figure 3*b* has three **C** components and

$$X = (x_a \quad x_b \quad x_c)^{\mathrm{T}}. \tag{3.26}$$

Following the same arguments as for figure 3*a*, it follows that

$$x = \begin{pmatrix} x_a \\ x_b \end{pmatrix} = L_{xX}X, \quad \text{where } L_{xX} = \begin{pmatrix} 1 & 0 & 0 \\ 0 & 1 & 0 \end{pmatrix} \tag{3.27}$$

and

$$X^d = (x_c) = L_{dX}X, \quad \text{where } L_{dX} = (0 \quad 0 \quad 1) \quad \text{and} \quad L_{dx} = (-1 \quad -1). \tag{3.28}$$

In this case,

$$G = L_{dX} - L_{dx}L_{xX} = (0 \quad 0 \quad 1) - (-1 \quad -1)\begin{pmatrix} 1 & 0 & 0 \\ 0 & 1 & 0 \end{pmatrix} = (1 \quad 1 \quad 1). \tag{3.29}$$

In this particular case, $G\dot{X} = 0$ corresponds to

$$\dot{x}_a + \dot{x}_b + \dot{x}_c = 0 \quad \text{or} \quad x_a + x_b + x_c = \text{const.} \tag{3.30}$$

Thus, the total amount of $A$, $B$ and $C$ is constant.

The system of figure 3*c* has four **C** components and

$$X = (x_a \quad x_b \quad x_c \quad x_d)^{\mathrm{T}}. \tag{3.31}$$

Following the same arguments as for figure 3*a*, it follows that

$$x = (x_a) = L_{xX}X, \quad \text{where } L_{xX} = (1 \quad 0 \quad 0 \quad 0) \tag{3.32}$$

and

$$X^d = (x_b \quad x_c \quad x_d)^{\mathrm{T}} = L_{dX}X, \tag{3.33}$$

where

$$L_{dX} = \begin{pmatrix} 0 & 1 & 0 & 0 \\ 0 & 0 & 1 & 0 \\ 0 & 0 & 0 & 1 \end{pmatrix} \quad \text{and} \quad L_{dx} = \begin{pmatrix} 1 \\ -1 \\ -1 \end{pmatrix}. \tag{3.34}$$

In this case,

$$G = L_{dX} - L_{dx}L_{xX} = \begin{pmatrix} 0 & 1 & 0 & 0 \\ 0 & 0 & 1 & 0 \\ 0 & 0 & 0 & 1 \end{pmatrix} - \begin{pmatrix} 1 \\ -1 \\ -1 \end{pmatrix}(1 \quad 0 \quad 0 \quad 0) = \begin{pmatrix} -1 & 1 & 0 & 0 \\ 1 & 0 & 1 & 0 \\ 1 & 0 & 0 & 1 \end{pmatrix}. \tag{3.35}$$

In this particular case, $G\dot{X} = 0$ corresponds to

$$x_b = x_a + \text{const.}, \quad x_a + x_c = \text{const.} \quad \text{and} \quad x_a + x_d = \text{const.}$$

Thus, the amount of $B$ equals the amount of $A$ plus a constant, the total amount of $A$ and $C$ is constant and the total amount of $A$ and $D$ is constant.

Continuing the analysis of the system of figure 3*b* but including the extra input of figure 3*d*, the flow vector has an extra component $v_0$ and can be defined as

$$V = (v_0 \quad v_1 \quad v_2)^{\mathrm{T}}, \tag{3.36}$$

where $v_1$ and $v_2$ are the two reaction flows. It is convenient to decompose $V$ into two components: $v$ the independent part of $V$ and $V^d$ part of $V$ dependent on $\dot{X}$ and $v$. In particular,

$$v = v_0 = K_{vV}V, \quad \text{where } K_{vV} = (1 \quad 0 \quad 0) \tag{3.37}$$

and

$$V^d = \begin{pmatrix} v_1 \\ v_2 \end{pmatrix} = K_{dV}V, \quad \text{where } K_{dV} = \begin{pmatrix} 0 & 1 & 0 \\ 0 & 0 & 1 \end{pmatrix}. \tag{3.38}$$

Moreover, following the causal strokes in figure 3*d* the flow vector $V$ can be written in terms of the state derivative $\dot{X}$ and the independent flow $v$ as

$$V = K_{VX}\dot{X} + K_{Vv}v, \tag{3.39}$$

where

$$K_{VX} = \begin{pmatrix} 0 & 0 & 0 \\ -1 & 0 & 0 \\ -1 & -1 & 0 \end{pmatrix} \quad \text{and} \quad K_{Vv} = \begin{pmatrix} 1 \\ 1 \\ 1 \end{pmatrix}. \tag{3.40}$$

In the particular case that the system is in a steady state and so $\dot{X} = 0$:

$$V = Kv, \quad \text{where } K = K_{Vv} \tag{3.41}$$

Substituting into equation (3.3) it follows that $NKv = 0$. As this must be true for all $v$, it follows that $NK = 0$ and thus $K$ is a right null matrix of $N$.

## (c) Reduced-order equations

The stoichiometric analysis of §3*a*,*b* has many uses; one of these, reducing the order of the ordinary differential equations (ODEs) describing a system,[7] is given here. Reducing system order gives a smaller set of equations to solve and may avoid numerical problems, for example, arising from failure to recognize conserved moieties in a reaction system.

From equation (3.18), the derivatives $\dot{X}^d$ of the dependent state $X^d$ can be written as linear transformation of the derivatives $\dot{x}$ of the independent state $x$ as

$$\dot{X}^d = L_{dx}\dot{x}. \tag{3.42}$$

Integrating this equation gives

$$X^d - X^d(0) = L_{dx}(x - x(0)), \tag{3.43}$$

where $X^d(0)$ and $x(0)$ are the values of $X^d$ and $x$ at time zero. Using equations (3.15), (3.16) and (3.21), equation (3.43) can be rewritten as

$$X^d = L_{dx}x + X^d(0) - L_{dx}x(0) = L_{dx}x + (L_{dX} - L_{dx}L_{xX})X(0) = L_{dx}x + GX(0). \tag{3.44}$$

Using equation (3.17) to reconstruct $X$ from $X^d$ given by equation (3.44) and $x$ gives

$$X = (L_{xX}^T + L_{dX}^T L_{dx})x + L_{dX}^T GX(0) = Lx + G_X X(0), \tag{3.45}$$

where

$$L = L_{xX}^T + L_{dX}^T L_{dx} \quad \text{and} \quad G_X = L_{dX}^T G. \tag{3.46}$$

Equation (3.44) gives an explicit expression for reconstructing the full state $X$ from the independent state $x$ and the initial state $X(0)$.

From equation (3.3), the state $X$ is given by the system ODE as

$$\dot{X} = NV(X, u), \tag{3.47}$$

where $u$ represents external flows (for example, $v$ in figure 3*d*). Using equations (3.15) and (3.45), the ODE in $X$ of equation (3.47) can be rewritten as the reduced order ODE in $x$ as

$$\dot{x} = L_{xX}NV(Lx + G_X X(0), u) \tag{3.48}$$

and the full state reconstructed using equation (3.45).

## 4. Model reduction and approximation of reaction mechanisms

As discussed in the Introduction, complex systems can be simplified by approximation. However, it is crucial that such approximation does not destroy the compliance with thermodynamic principles reflected in the original system.

---

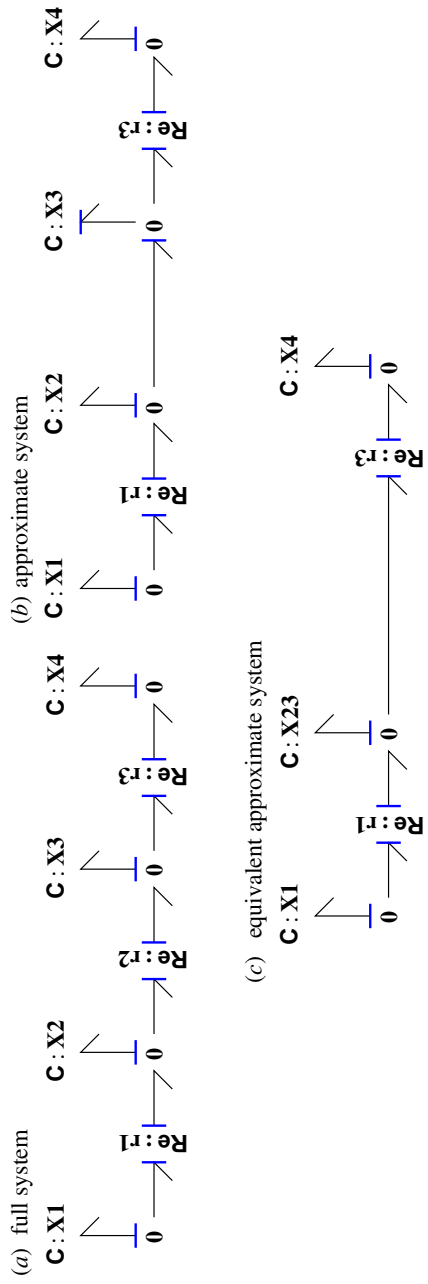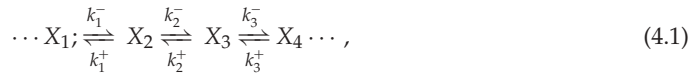[7]Order reduction is also discussed in [63–67].

**Figure 4.** Approximation of unimolecular reactions [26, §3.1]. The reaction chain (*a*) is approximated in (*b*) by assuming that the reaction represented by **Re** : **r2** is fast ($1/\kappa_2 \approx 0$) and so may be removed. (*c*) is exactly equivalent to (*b*) except that the adjacent **C** : **X2** and **C** : **X3** are replaced by the composite component **C** : **X23** with coefficient $\kappa_{23}$ given by equation (4.12). (Online version in colour.)

15

rspa.royalsocietypublishing.org  *Proc. R. Soc. A* **470**: 20140459

In their analysis of the sodium pump, which transports sodium ions out of electrically excitable cells such as cardiomyocytes, Smith & Crampin [26] consider simplification of the linear chain of reactions:

$$\cdots X_1; \underset{k_1^+}{\overset{k_1^-}{\rightleftharpoons}} X_2 \underset{k_2^+}{\overset{k_2^-}{\rightleftharpoons}} X_3 \underset{k_3^+}{\overset{k_3^-}{\rightleftharpoons}} X_4 \cdots, \tag{4.1}$$

where the middle reaction in the chain is fast relative to the other reactions. The three reactions have flows $v_1 \ldots v_3$ given by

$$v_1 = k_1^+ X_1 - k_1^- X_2, \quad v_2 = k_2^+ X_2 - k_2^- X_3 \quad \text{and} \quad v_3 = k_3^+ X_3 - k_3^- X_4. \tag{4.2}$$

Reaction (4.1) corresponds to the bond graph of figure 4a which has the flows of equations (4.2), where

$$k_1^+ = \kappa_1 K_1, \quad k_1^- = \kappa_1 K_2, \tag{4.3}$$

$$k_2^+ = \kappa_2 K_2, \quad k_2^- = \kappa_2 K_3, \tag{4.4}$$

and
$$k_3^+ = \kappa_3 K_3, \quad k_3^- = \kappa_3 K_4. \tag{4.5}$$

If $\kappa_2 \gg \kappa_1$ and $\kappa_2 \gg \kappa_3$, equation (4.4) can be rewritten as

$$\kappa_2 = \frac{1}{\epsilon}, \tag{4.6}$$

where $\epsilon$ is a small positive number. $v_2$ (4.2) and (4.4) can then be rewritten as

$$\epsilon v_2 = K_2 X_2 - K_3 X_3 \tag{4.7}$$

assuming non-zero $v_2$ this means that as $\epsilon \to 0$, $X_2$ and $X_3$ are in equilibrium and

$$X_3 = \rho X_2, \quad \text{where } \rho = \frac{K_2}{K_3}. \tag{4.8}$$

This also means that the difference in affinities associated with reaction 2 is zero

$$A_2^f - A_2^r = K_2 X_2 - K_3 X_3 = 0. \tag{4.9}$$

Thus, the corresponding reaction component **Re** : **r3** can be removed from the bond graph to give figure 4b. This implies that the **C** : **X3** component is in derivative causality and thus the bond graph represents a differential-algebraic equation and an ordinary differential equation. However, as discussed by Gawthrop & Bevan [11], as **C** : **X2** and **C** : **X3** are on adjacent **0** junctions, they may be replaced by the single **C** : **X23** component as in figure 4c.

Figure 4c represents the same system as figure 4b if **C** : **X23** contains the same molar mass as **C** : **X2** and **C** : **X3**. Moreover, using equations (4.8)

$$X_{23} = X_2 + X_3 = (1 + \rho) X_2. \tag{4.10}$$

The equilibrium constant $K_{23}$ of **C** : **X23** must also correspond to those of **C** : **X2** and **C** : **X3** so that

$$K_2 X_2 = K_3 X_3 = K_{23} X_{23} \tag{4.11}$$

hence

$$K_{23} = \frac{K_2}{1 + \rho} = \frac{\rho K_3}{1 + \rho}. \tag{4.12}$$

The bond graph of figure 4c corresponds to the reaction scheme [26, §3.1]:

$$\cdots X_1 \underset{\alpha_1^-}{\overset{\alpha_1^+}{\rightleftharpoons}} X_{23} \underset{\alpha_3^-}{\overset{\alpha_3^+}{\rightleftharpoons}} X_4 \cdots \tag{4.13}$$

where

$$\alpha_1^+ = \kappa_1 K_1 = k_1^+ \quad \alpha_1^- = \kappa_1 K_{23} = \kappa_1 \frac{K_2}{1+\rho} = \frac{k_1^-}{1+\rho} \left.\begin{array}{c} \\ \\ \\ \end{array}\right\}$$

$$\text{and} \qquad \alpha_3^+ = \kappa_3 K_{23} = \kappa_1 \frac{\rho K_3}{1+\rho} = \frac{\rho k_3^+}{1+\rho} = \frac{k_3^+}{1+(1/\rho)} \quad \alpha_3^- = \kappa_3 K_4 = k_3^-. \tag{4.14}$$

Noting that '$K_2$' in Smith & Crampin [26, §3.1] corresponds to '$\rho$' in this paper, equations (4.14) correspond to eqn (18) of Smith & Crampin [26].

In general, a chain of $N$ **C** components and $N-1$ **Re** components where all of the reactions are fast may be approximately replaced by a single **C** component with

$$K = \frac{1}{1/K_1 + 1/K_2 \ldots 1/K_N} = \frac{1}{\sum_{i=1}^{N}(1/K_i)}. \tag{4.15}$$

This procedure is extended to bimolecular reactions in the electronic supplementary material, §B.

## 5. Biochemical cycles

Many biochemical processes central to cellular physiology represent biochemical cycles: including enzyme catalysed reactions, transport processes and signalling cascades. A very simple, but practically important, biochemical cycle is the enzyme-catalysed reaction of figure 1*f*. This reaction is closely related to that of figure 1*d* with the important difference that the enzyme $E$ appears on both sides of the reaction creating the 'loop' in the bond graph corresponding to a biochemical cycle. Moreover, in figure 1*f*, the net flow into $E$ is zero and thus $\dot{x}_e = 0$ and $x_e = e_0$, where $e_0$ is a constant. It follows that

$$v = \kappa(K_e x_e K_s x_s - K_e x_e K_p x_p) = \kappa_e(K_s x_s - K_p x_p), \tag{5.1}$$

where

$$\kappa_e = \kappa K_e e_0. \tag{5.2}$$

### (a) Example: enzyme-catalysed reaction cycles

As noted above, the enzyme-catalysed reaction of figure 1*f* simplifies to a simple reaction with a modified reaction constant $\kappa_e = \kappa K_e e_0$. However, it is known from experiments that this simple model of an enzyme-catalysed reaction fails for high reaction flows. For this reason, as discussed in [2,3,15], an intermediate complex $C$ is introduced so that the reaction

$$S + E \rightleftharpoons P + E \tag{5.3}$$

is replaced by

$$S + E \overset{1}{\rightleftharpoons} C \overset{2}{\rightleftharpoons} P + E. \tag{5.4}$$

This reaction may then be replaced by various versions of the Michaelis–Menten approximation. As discussed by Gunawardena [6], this approximation has been much misused. In particular, it is used in circumstances which violate the fundamental law of thermodynamics.

Using the bond graph approach, this section derives a Michaelis–Menten approximation which is thermodynamically compliant. In particular, the aim of the approximation is, as for the simple case of figure 1*f*, to replace the enzyme-catalysed reaction by a single **Re** component with an equivalent gain $\kappa_e$. But, unlike the simple case, $\kappa_e$ is not a constant but rather an nonlinear function of the forward and backward affinities.

Figure 5*a* shows the enzyme-catalysed reaction (with complex $C$). The substrate $S$ and product $P$ are omitted from the bond graph as they do not form part of the approximation. This is a more general approach than usual as the result to be derived holds for any biochemical network giving rise to $A^f$ and $A^r$. As already stated, the aim of the approximation is to replace the bond graph
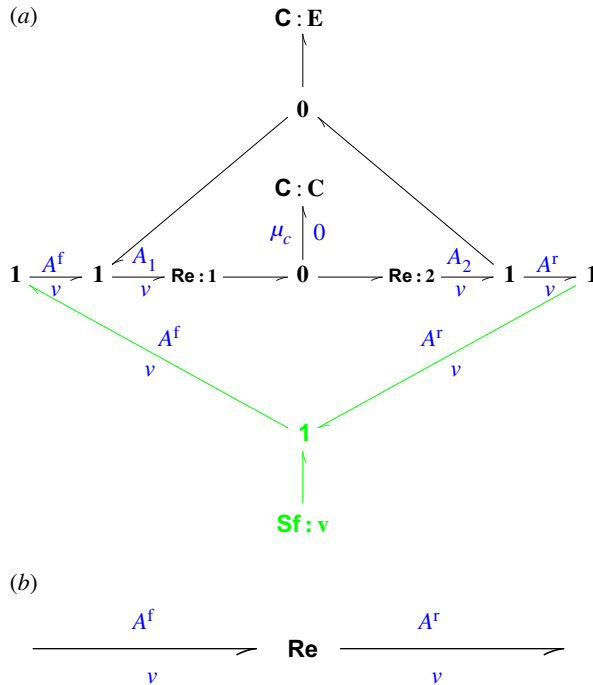
**Figure 5.** (*a*,*b*) The Michaelis–Menten approximation: (*a*) full, (*b*) approximate. (Online version in colour.)

of figure 5*a* by a single **Re** component of figure 5*b*. As, by definition, the **Re** component has the same flow on each port, it is natural to approximate the bond graph of figure 5*a* by enforcing this constraint at the outset. To do this, the flow component **Sf** : **v** is used to impose a flow $v$ on each port thus generating the corresponding forward $A^f$ and backward $A^r$ affinities.

With reference to figure 5*a*, and using equation (2.6), the equation describing the left-hand **Re** component may be rewritten as

$$e^{A_1/RT} = e^{\mu_c/RT} + \frac{v}{\kappa_1} = K_c x_c + \frac{v}{\kappa_1} \tag{5.5}$$

hence

$$A_1 = RT \ln \left( K_c x_c + \frac{v}{\kappa_1} \right) \quad \text{and} \quad A_2 = RT \ln \left( K_c x_c - \frac{v}{\kappa_1} \right). \tag{5.6}$$

It follows that $A^f$ is given by

$$A^f = A_1 - \mu_e = A_1 - RT \ln K_e x_e = RT \ln \frac{K_c x_c + v/\kappa_1}{K_e x_e} \tag{5.7}$$

and, similarly

$$A^r = RT \ln \frac{K_c x_c - v/\kappa_1}{K_e x_e}. \tag{5.8}$$

It is convenient to transform $A^f$ and $A^r$ into $v_0^+$ and $v_0^-$, where:

$$v_0^+ = e^{A^f/RT} \quad \text{and} \quad v_0^- = e^{A^r/RT} \tag{5.9}$$

giving

$$v_0^+ = \frac{K_c x_c + v/\kappa_1}{K_e x_e} \quad \text{and} \quad v_0^- = \frac{K_c x_c - v/\kappa_2}{K_e x_e}. \tag{5.10}$$

Subtracting these equations gives

$$v_0^+ - v_0^- = \frac{1/\kappa_1 + 1/\kappa_2}{K_e x_e} v \tag{5.11}$$

hence

$$v = \bar{\kappa} K_e x_e \delta_v, \quad \text{where } \bar{\kappa} = \frac{\kappa_1 \kappa_2}{\kappa_1 + \kappa_2} \quad \text{and} \quad \delta_v = v_0^+ - v_0^-. \tag{5.12}$$

Multiplying equations (5.10) by $\kappa_1$ and $\kappa_2$, respectively, and adding gives

$$\kappa_1 v_0^+ + \kappa_2 v_0^- = (\kappa_1 + \kappa_2) \frac{K_c x_c}{K_e x_e} \tag{5.13}$$

hence

$$x_c = \frac{K_e}{K_c} \sigma_v x_e, \quad \text{where } \sigma_v = \frac{\kappa_1 v_0^+ + \kappa_2 v_0^-}{\kappa_1 + \kappa_2} = \frac{\kappa_1 \, e^{A^f/RT} + \kappa_2 \, e^{A^r/RT}}{\kappa_1 + \kappa_2}. \tag{5.14}$$

Using the feedback loop implied by $x_e = e_0 - x_c$ and equation (5.14)

$$x_e = \frac{e_0}{1 + (K_e/K_c)\sigma_v}. \tag{5.15}$$

Substituting equation (5.15) into equation (5.12) gives

$$v = \bar{\kappa} \frac{K_e e_0}{1 + (K_e/K_c)\sigma_v} \delta_v = \bar{\kappa} \frac{K_c e_0}{K_c/K_e + \sigma_v} \delta_v. \tag{5.16}$$

There are two special cases of interest $\kappa_1 = \kappa_2$ and $\kappa_1 \gg \kappa_2$. In these two cases, $\sigma_v$ is given by

$$\sigma_v = \begin{cases} \dfrac{v_0^+ + v_0^-}{2} = \dfrac{e^{A^f/RT} + e^{A^r/RT}}{2} & \kappa_1 = \kappa_2 \\ v_0^+ = e^{A^f/RT} & \kappa_1 \gg \kappa_2. \end{cases} \tag{5.17}$$

Hence the enzyme-catalysed reaction can be approximated by the **Re** component with equivalent gain $\kappa_e$ given by

$$\kappa_e = e_0 \frac{\bar{\kappa} K_c}{k_m + \sigma_v}, \quad \text{where } k_m = \frac{K_c}{K_e}. \tag{5.18}$$

In contrast to the expression for the simple case (5.2) $\kappa_e$ is, via $\sigma_v$ (5.17), a function of the affinities $A^f$ and $A^r$. The fact that $\sigma_v > 0$ ensures that the **Re** component corresponding to equation (5.18) is thermodynamically compliant.
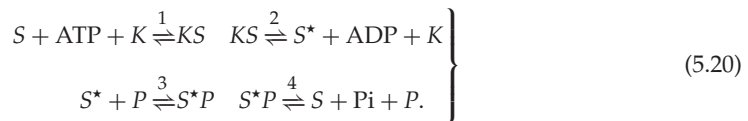
In both equations (5.2) and (5.18), the expression for $\kappa_e$ has a factor $e_0$, the (constant) sum of $x_e$ and $x_c$. In many biochemical situations, the enzyme $E$ is the product of another reaction. Although equation (5.18) is derived for a constant $e_0$, a further approximation would be to allow $e_0$ to be time varying $e_0 = x_E$ where $x_E$ is the enzyme concentration from an external reaction. This leads to the concept of the *modulated* **Re**, or **mRe** component of figure 5c. The additional modulating bond carries two signals: the effort $\mu_E$, where

$$\mu_E = e^{x_e/RT} \tag{5.19}$$

and a zero flow. The zero flow means that the modulating bond does *not* transmit power. The **mRe** component is used to approximate the system of §5b.

## (b) Example: a biochemical switch

Beard & Qian [2, §5.1.1] discuss a biochemical switch described by

$$\left. \begin{aligned} S + \text{ATP} + K \overset{1}{\rightleftharpoons} KS \quad KS \overset{2}{\rightleftharpoons} S^\star + \text{ADP} + K \\[4pt] \text{and} \qquad\qquad S^\star + P \overset{3}{\rightleftharpoons} S^\star P \quad S^\star P \overset{4}{\rightleftharpoons} S + \text{Pi} + P. \end{aligned} \right\} \tag{5.20}$$

These reactions represent a phosphorylation/dephosphorylation cycle. Protein $S$ is phosphorylated by kinase $K$ and is dephosphorylated by phosphatase $P$, where $S^\star$ represents the phosphorylated (active, perhaps) state of the protein. The corresponding bond graph appears in figure 6a where the external flow $v_a$ necessary to top up the ATP reservoir is included. This system contains nine states and four reactions with mass-action kinetics. Using the approximation of §5a,
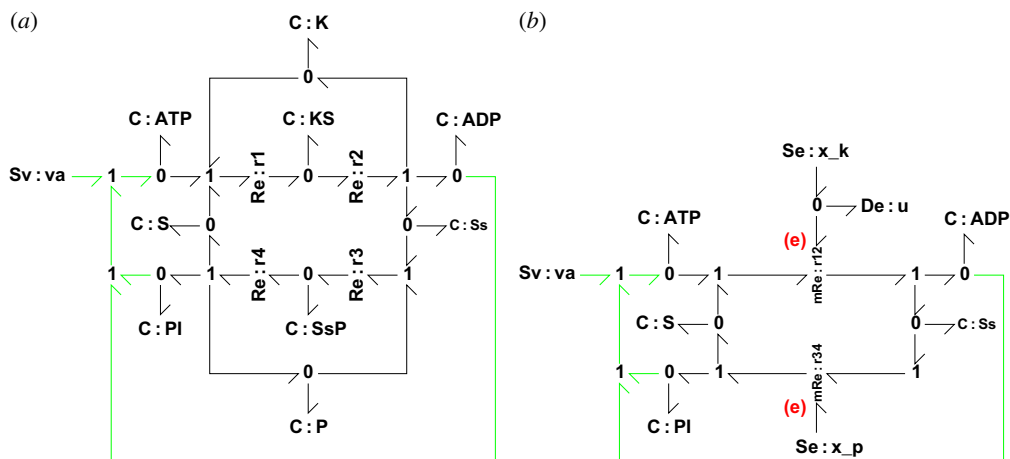
**Figure 6.** A biochemical switch. (*a*) The bond graph of the biochemical switch of Beard & Qian [2] has four reactions **Re** : **r1**–**Re** : **r4** and nine substances. The external flow $v_a$ of ATP is required for the long-term operation of the switch which consumes ATP. (*b*) This switch can be approximated using the approximation of figure 5 while retaining thermodynamic compliance. (Online version in colour.)

figure 5, this system can be approximated by the bond graph of 6*b*. The approximate system has five states and two reactions with the reversible Michaelis–Menten kinetics of §5*a*. It has the further advantage that the dynamics are explicitly modulated by the concentrations $x_k$ and $x_p$ of *K* and *P*, respectively.

The bond graph of 6*b* clearly shows a biochemical cycle. Its behaviour can be understood as follows. When $x_k$ is large, ATP drives *S* though the reaction component **Re** : **r12** to create $S^\star$; and this flow is greater than that though **Re** : **r34** and so the amount of $S^\star$ increases at the expense of *S*. However, when $x_k$ is small the flow though **Re** : **r12** becomes less than that though **Re** : **r34** and amount of $S^\star$ decreases.

For the purposes of illustration, the following parameter values were used. With reference to equation (5.18), $k_m = 0$ and $\bar{\kappa} K_c = 100$ for both reactions. With reference to equations (2.3), $K_{\mathrm{ATP}} = 10$ and $K_S = K_{S*} = K_{\mathrm{ADP}} = K_{\mathrm{PI}} = 1$. The initial states were $x_{\mathrm{ATP}} = 10$, $x_S = x_{\mathrm{ADP}} = 1$ and $x_{S*} = x_{\mathrm{PI}} = 0$.

Figure 7 shows a simulation of the biochemical switch when ATP is replenished by setting

$$v_a = g_a(w_{\mathrm{ATP}} - x_{\mathrm{ATP}}), \quad \text{where } g_a = 2 \quad \text{and} \quad w_{\mathrm{ATP}} = 10. \tag{5.21}$$

Equation (5.21) represents simple proportional feedback; *in vivo*, this would correspond to a cellular control system. Figure 7*a* shows the response of the amount of $S^\star$ to a sinusoidal variation in the amount of *K*. The biochemical switch both amplifies and distorts the signal. This effect is further shown in figure 7*b* where the amount of $S^\star$ is plotted against the amount of *K*. This is basically a high-gain saturating function. The hysteresis is due to the time constant of the feedback loop implied by equation (5.21); the hysteresis reduces if either $g_a$ is increases or the frequency of the input sinusoid decreased. All biochemical cycles require free-energy transduction [1]. Figure 7*c* shows the molar flow of ATP into the system (and, as indicated in figure 6*b*, the outflow of ADP and Pi) as a function of time; the ON state of the switch induces a flow of ATP using equation (5.21) to replenish the ATP consumed by the cycle. Figure 7*d* shows the corresponding amounts of ATP, ADP and Pi. The controller does not exactly hold ATP at the desired level of $w_{\mathrm{ATP}} = 10$; a higher gain controller would reduce the control error. As discussed by Beard & Qian [2, §5.1.1]: '. . . a biochemical switch cannot function without a free energy input. No energy, no switch'. This can be simulated by setting $g_a = 0$ in equation (5.21) and forms the electronic supplementary material, figure S1 of §A.
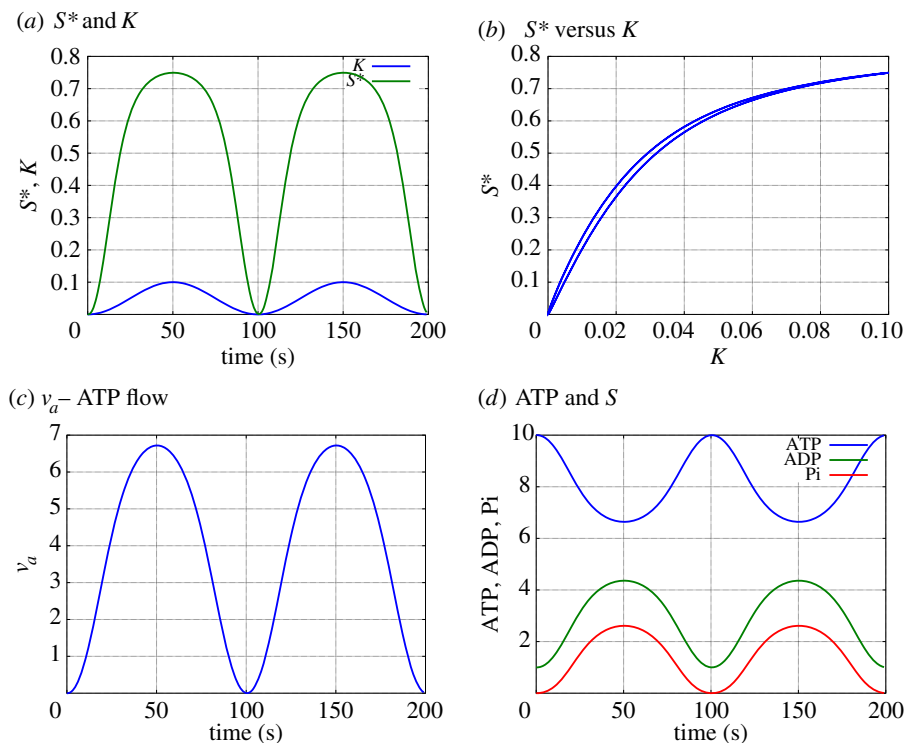
**Figure 7.** A biochemical switch: simulation. (*a*) The time response of the amount of $S^\star$ to a sinusoidal variation in the amount of $K$. The biochemical switch both amplifies and distorts the signal. Panel (*b*) plots $S^\star$ against $K$ to show the nonlinear amplification effect. (*c*) The corresponding molar flow of ATP into the system and (*d*) the corresponding amounts of ATP, ADP and Pi. (Online version in colour.)

Approximate models of signalling network components have been advocated by Kraeutler *et al.* [68] and Ryall *et al.* [69] as an approach to understanding the behaviour of complex signalling networks. The models developed in this section could also be used for such a purpose, but with the advantage that the resulting model is thermodynamically compliant.

Model reduction of an enzymatic cycle model of the SERCA pump [70] is discussed in the electronic supplementary material, §c.

# 6. Hierarchical modelling of large systems

One of the objectives of systems biology is to represent the network of biochemical reactions taking place in cells by computational models. Large-scale models of cellular metabolic and signalling networks have been constructed; for example, cardiac cell models which integrate electrophysiology, metabolism, signalling and cellular mechanics have been developed in order to study cell physiology in normal and disease conditions [71].

In order to facilitate the development and reuse of such models, XML-based markup languages such as CellML [72] and SBML [73] have been created. These languages enable mathematical descriptions of biological processes to be stored in machine-readable formats, but put relatively little restriction on the formulation of the models themselves.

For example, CellML, which was originally developed in order to share models of cardiac cell dynamics, represents models as a number of component elements, each of which contains a number of variables (for example, representing cell membrane potential, or an ionic concentration), the mathematical relationship between these variables (for example, the Nernst

potential given as a function of the concentrations) expressed in MathML, and associated parameters. Such components can be connected to one another to form a model.

This construction allows a modular approach to modelling in which cellular processes and reactions can be broken down into components, which are then connected to form a model of the system under study [74]. However, there is no requirement that components adhere to the principles of conservation of mass, conservation of charge or thermodynamic consistency. Nor is there currently any framework which would ensure thermodynamic consistency, or mass or charge conservation, for a model created by connecting components in this modular fashion, even if the components themselves were constructed as thermodynamic cycles.

The bond graph approach which we have outlined here provides such a framework for modular representation of components of biological systems, which can be assembled so as to preserve thermodynamic properties, charge and mass conservation, both in the individual components and in the overall system. Furthermore, the development of the bond graph markup language (BGML) by Borutzky [35] for the exchange and reuse of bond graph models, and associated software, provides the tools through which integration with representations such as CellML may be achieved.

The stoichiometric analysis of §3, and its relationship to causality, is illustrated by simple systems. However, the notion of bond graph causality, and the corresponding propagation of causality using the *sequential causality assignment procedure* [10, ch. 5], is applicable to arbitarily large systems.

## 7. Conclusion

Based on the seminal work of Oster *et al.* [16], the fundamental concepts of network thermodynamics have been combined with more recent developments in the bond graph approach to system modelling to give a new approach to building dynamical models of biochemical networks within which compliance with thermodynamic principles is automatically satisfied. As noted in the Introduction, the bond graph is more than a sketch of a biochemical network; it can be directly interpreted by a computer and, moreover, has a number of features that enable key physical properties to be derived from the bond graph itself. It has been shown that stoichiometric properties, including the stoichiometric matrix $N$ and the left and right null-space matrices $G$ and $K$, can be directly derived from the bond graph using the concept of causality associated with bond graphs. The corresponding causal paths, when superimposed on the bond graph, directly indicate both pools (conserved moieties) and steady-state flux paths. The bond graph methodology includes a framework for approximating complex systems while retaining compliance with thermodynamic principles and this has been illustrated in two contexts: chains of reactions and the Michaelis–Menten approximation of enzyme-catalysed reactions.

As emphasized by Beard & Qian [2], living organisms are associated with *non-equilibrium* steady states. For this reason, this paper has emphasized the role of external inputs to biochemical networks modelled by bond graphs. In particular, the example of §5*b*, models a biochemical switch where the role of ATP as a power source is explicitly integrated into the bond graph model.

The bond graph approach is naturally modular in that networks of biochemical reactions can be connected by bonds while retaining compliance with thermodynamic principles. Modularity has been illustrated by simple examples and future work will develop appropriate software tools to build on this natural modularity.

Biochemical networks have nonlinear dynamics which generate phenomena which cannot be generated by linear systems. Nevertheless, useful information can be obtained from linear models obtained by linearization of nonlinear systems. In the context of engineering systems theory, linearization has been considered within the framework of sensitivity theory [75,76]. In the context of biochemical networks, metabolic control analysis (MCA) [77] is based on the sensitivity analysis of stoichiometric networks. The relationship of MCA to engineering concepts of sensitivity has been examined by Ingalls & Sauro [64], Ingalls [65] and Sauro [66]. Ingalls [65] has shown that standard engineering sensitivity theory can be applied to biochemical networks to

derive frequency responses with respect to small perturbations in system parameters. Sensitivity and linearization of systems described by bond graphs has been considered in earlier studies [78–80]. The bond graph approach has the advantage of retaining the system structure. Future work will look at bond graph-based linearization in the context of biochemical networks.

This paper has focused on deriving thermodynamically compliant biochemical reaction networks, and their thermodynamically compliant approximations, from elementary biochemical equations. It would be interesting to look at the inverse problem: Is a given ODE model of a system of biochemical reactions with non-mass-action kinetics thermodynamically compliant and does it have a bond graph representation?

In addition to stoichiometric analysis, the bond graph approach can be used to directly investigate structural properties of dynamical systems such as controllability [62,81] and invertibility [59,61,82,83]. Future work will look at bond graph-based structural analysis in the context of biochemical networks.

The bond graph approach is based on the notion of power flow. For this reason, it has been much used for modelling multi-domain engineering systems with appropriate transducer models to interface domains. Thus, for example: an electric motor or a piezo-electric actuator couples electrical and mechanical domains and a turbine or pump couples hydraulic and mechanical domains. We will build on the work of LeFèvre *et al.* [43] on chemo-mechanical transduction and the work of Karnopp [39] on chemo-electrical transduction to interface biochemical networks with systems involving muscle and excitable membranes.

We believe that, when combined with modern software tools, the bond graph approach provides a significant alternative hierarchical and modular modelling framework for complex biochemical systems in which compliance with thermodynamic principles is automatically satisfied.

# References

1. Hill TL. 1989 *Free energy transduction and biochemical cycle kinetics*. New York, NY: Springer.
2. Beard DA, Qian H. 2010 *Chemical biophysics: quantitative analysis of cellular systems*. Cambridge, UK: Cambridge University Press.
3. Keener JP, Sneyd J. 2009 *Mathematical physiology: I: cellular physiology*, vol. 1, 2nd edn. Berlin, Germany: Springer.
4. Katchalsky A, Curran PF. 1965 *Nonequilibrium thermodynamics in biophysics*. Cambridge, MA: Harvard University Press.
5. Cellier FE. 1991 *Continuous system modelling*. Berlin, Germany: Springer.
6. Gunawardena J. 2014 Time-scale separation—Michaelis and Menten's old idea, still bearing fruit. *FEBS J.* **281**, 473–488. (doi:10.1111/febs.12532)
7. Paynter HM. 1992 An epistemic prehistory of bond graphs. In *Bond graphs for engineers* (eds PC Breedveld, G Dauphin-Tanguy), pp. 3–17. Amsterdam, The Netherlands: North-Holland.
8. Gawthrop PJ, Smith LPS. 1996 *Metamodelling: bond graphs and dynamic systems*. Hemel Hempstead, UK: Prentice Hall.
9. Borutzky W. 2011 *Bond graph modelling of engineering systems: theory, applications and software support*. Berlin, Germany: Springer.
10. Karnopp DC, Margolis DL, Rosenberg RC. 2012 *System dynamics: modeling, simulation, and control of mechatronic systems*, 5th edn. New York, NY: John Wiley & Sons.
11. Gawthrop PJ, Bevan GP. 2007 Bond-graph modeling: a tutorial introduction for control engineers. *IEEE Control Syst. Mag.* **27**, 24–45. (doi:10.1109/MCS.2007.338279)

12. Palsson B. 2006 *Systems biology: properties of reconstructed networks*. Cambridge, UK: Cambridge University Press.

13. Palsson B. 2011 *Systems biology: simulation of dynamic network states*. Cambridge, UK: Cambridge University Press.

14. Alon U. 2007 *Introduction to systems biology: design principles of biological networks*. Boca Raton, FL: CRC Press.

15. Klipp E, Liebermeister W, Wierling C, Kowald A, Lehrach H, Herwig R. 2011 *Systems biology*. New York, NY: Wiley-Blackwell.

16. Oster G, Perelson A, Katchalsky A. 1971 Network thermodynamics. *Nature* **234**, 393–399. (doi:10.1038/234393a0)

17. Oster GF, Perelson AS, Katchalsky A. 1973 Network thermodynamics: dynamic modelling of biophysical systems. *Q. Rev. Biophys.* **6**, 1–134. (doi:10.1017/S0033583500000081)

18. Oster G, Perelson A. 1974 Chemical reaction networks. *Circuits Syst. IEEE Trans.* **21**, 709–721. (doi:10.1109/TCS.1974.1083946)

19. Oster GF, Auslander DM. 1971 Topological representations of thermodynamic systems—I. Basic concepts. *J. Franklin Inst.* **292**, 1–17. (doi:10.1016/0016-0032(71)90037-8)

20. Oster GF, Auslander DM. 1971 Topological representations of thermodynamic systems—II. Some elemental subunits for irreversible thermodynamics. *J. Franklin Inst.* **292**, 77–92. (doi:10.1016/0016-0032(71)90196-7)

21. Kohl P, Crampin EJ, Quinn TA, Noble D. 2010 Systems biology: an approach. *Clin. Pharmacol. Ther.* **88**, 25–33. (doi:10.1038/clpt.2010.92)

22. Aldridge BB, Burke JM, Lauffenburger DA, Sorger PK. 2006 Physicochemical modelling of cell signalling pathways. *Nat. Cell. Biol.* **8**, 1195–1203. (doi:10.1038/ncb1497)

23. Smith NP, Crampin EJ, Niederer SA, Bassingthwaighte JB, Beard DA. 2007 Computational biology of cardiac myocytes: proposed standards for the physiome. *J. Exp. Biol.* **210**, 1576–1583. (doi:10.1242/jeb.000133)

24. Hunter PJ, Crampin EJ, Nielsen PMF. 2008 Bioinformatics, multiscale modeling and the IUPS Physiome Project. *Brief. Bioinform.* **9**, 333–343. (doi:10.1093/bib/bbn024)

25. Hunter P *et al.* 2012 The VPH-Physiome Project: standards, tools and databases for multi-scale physiological modelling. In *Modeling of physiological flows* (eds D Ambrosi, A Quarteroni, G Rozza), pp. 1–23. Italia: Springer.

26. Smith NP, Crampin EJ. 2004 Development of models of active ion transport for whole-cell modelling: cardiac sodium–potassium pump as a case study. *Progr. Biophys. Mol. Biol.* **85**, 387–405. (doi:10.1016/j.pbiomolbio.2004.01.010)

27. Tran K, Smith NP, Loiselle DS, Crampin EJ. 2009 A thermodynamic model of the cardiac sarcoplasmic/endoplasmic $Ca^{2+}$ (SERCA) pump. *Biophys. J.* **96**, 2029–2042. (doi:10.1016/j.bpj.2008.11.045)

28. Beard DA. 2005 A biophysical model of the mitochondrial respiratory system and oxidative phosphorylation. *PLoS Comput. Biol.* **1**, e36. (doi:10.1371/journal.pcbi.0010036)

29. Beard DA, Babson E, Curtis E, Qian H. 2004 Thermodynamic constraints for biochemical networks. *J. Theor. Biol.* **228**, 327–333. (doi:10.1016/j.jtbi.2004.01.008)

30. Beard DA, Liang S, Qian H. 2002 Energy balance for analysis of complex metabolic networks. *Biophys. J.* **83**, 79–86. (doi:10.1016/S0006-3495(02)75150-3)

31. Feist AM, Henry CS, Reed JL, Krummenacker M, Joyce AR, Karp PD, Broadbelt LJ, Hatzimanikatis V, Palsson BO. 2007 A genome-scale metabolic reconstruction for *Escherichia coli* K-12 MG1655 that accounts for 1260 ORFs and thermodynamic information. *Mol. Syst. Biol.* **3**, 121. (doi:10.1038/msb4100155)

32. Soh KC, Hatzimanikatis V. 2010 Network thermodynamics in the post-genomic era. *Curr. Opin. Microbiol.* **13**, 350–357. (doi:10.1016/j.mib.2010.03.001)

33. Ballance DJ, Bevan GP, Gawthrop PJ, Diston DJ. 2005 Model transformation tools (MTT): the open source bond graph project. In *Proc. 2005 Int. Conf. On Bond Graph Modeling and Simulation* (*ICBGM'05*), Simulation Series, pp. 123–128, New Orleans, LA: Society for Computer Simulation.

34. Cellier FE, Nebot A. 2005 The modelica bond graph library. In *Proc. 4th Int. Modelica Conf., Hamburg, Germany*, vol. 1, pp. 57–65. Modelica Association.

35. Borutzky W. 2006 BGML—a novel XML format for the exchange and the reuse of bond graph models of engineering systems. *Simul. Model. Practice Theory* **14**, 787–808. (doi:10.1016/j.simpat.2006.01.002)

36. Cellier FE, Greifeneder J. 2008 Thermobondlib—a new modelica library for modeling convective flows. In *Proc. 6th Int. Modelica Conf., Bielefeld, Deutschland*, pp. 163–172. Modelica Association.

37. Cellier FE, Greifeneder J. 2009 Modeling chemical reactions in modelica by use of chemo-bonds. In *Proc. 7th Modelica Conf., Como, Italy*. Modelica Association.

38. de la Calle A, Cellier FE, Yebra LJ, Dormido S. 2013 Improvements in bondlib the modelica bond graph library. In *Proc. 8th EUROSIM Congress, Cardiff, Cardiff, Wales*. Federation of European Simulation Societies.

39. Karnopp D. 1990 Bond graph models for electrochemical energy storage: electrical, chemical and thermal effects. *J. Franklin Inst.* **327**, 983–992. (doi:10.1016/0016-0032(90)90073-R)

40. Thoma JU, Atlan H. 1977 Network thermodynamics with entropy stripping. *J. Franklin Inst.* **303**, 319–328. (doi:10.1016/0016-0032(77)90114-4)

41. Greifeneder J, Cellier FE. 2012 Modeling chemical reactions using bond graphs. In *Proc. ICBGM12, 10th SCS Intl. Conf. on Bond Graph Modeling and Simulation, Genoa, Italy*, pp. 110–121. Society for Modeling and Simulation International.

42. Thoma J, Atlan H. 1985 Osmosis and hydraulics by network thermodynamics and bond graphs. *J. Franklin Inst.* **319**, 217–226. (doi:10.1016/0016-0032(85)90075-4)

43. LeFèvre J, LeFèvre L, Couteiro B. 1999 A bond graph model of chemo-mechanical transduction in the mammalian left ventricle. *Simul. Practice Theory* **7**, 531–552. (doi:10.1016/S0928-4869(99)00023-3)

44. Fuchs HU. 1996 *The dynamics of heat*. New York, NY: Springer.

45. Job G, Herrmann F. 2006 Chemical potential—a quantity in search of recognition. *Eur. J. Phys.* **27**, 353–371. (doi:10.1088/0143-0807/27/2/018)

46. Cellier FE. 1992 Hierarchical non-linear bond graphs: a unified methodology for modeling complex physical systems. *SIMULATION* **58**, 230–248. (doi:10.1177/003754979205800404)

47. Gawthrop PJ, Smith L. 1992 Causal augmentation of bond graphs with algebraic loops. *J. Franklin Inst.* **329**, 291–303. (doi:10.1016/0016-0032(92)90035-F)

48. Sueur C, Dauphin-Tanguy G. 1991 Bond graph approach to multi-time scale systems analysis. *J. Franklin Inst.* **328**, 1005–1026. (doi:10.1016/0016-0032(91)90066-C)

49. Qian H, Beard DA. 2005 Thermodynamics of stoichiometric biochemical networks in living systems far from equilibrium. *Biophys. Chem.* **114**, 213–220. (doi:10.1016/j.bpc.2004.12.001)

50. Qian H, Beard DA, Liang S-D. 2003 Stoichiometric network theory for nonequilibrium biochemical systems. *Eur. J. Biochem.* **270**, 415–421. (doi:10.1046/j.1432-1033.2003.03357.x)

51. Van Rysselberghe P. 1958 Reaction rates and affinities. *J. Chem. Phys.* **29**, 640–642. (doi:10.1063/1.1744552)

52. Boudart M. 1983 Thermodynamic and kinetic coupling of chain and catalytic reactions. *J. Phys. Chem.* **87**, 2786–2789. (doi:10.1021/j100238a018)

53. Laidler KJ. 1985 René Marcelin (1885–1914), a short-lived genius of chemical kinetics. *J. Chem. Edu.* **62**, 1012. (doi:10.1021/ed062p1012)

54. Jamshidi N, Palsson B. 2011 Metabolic network dynamics: properties and principles. In *Understanding the dynamics of biological systems* (eds J Southgate, W Dubitzky, H Fuß), pp. 19–37. Berlin, Germany: Springer. (doi:10.1007/978-1-4419-7964-3_2)

55. Schilling CH, Letscher D, Palsson B. 2000 Theory for the systemic definition of metabolic pathways and their use in interpreting metabolic function from a pathway-oriented perspective. *J. Theor. Biol.* **203**, 229–248. (doi:10.1006/jtbi.2000.1073)

56. Schuster S, Hilgetag C, Woods JH, Fell DA. 2002 Reaction routes in biochemical reaction systems: algebraic properties, validated calculation procedure and example from nucleotide metabolism. *J. Math. Biol.* **45**, 153–181. (doi:10.1007/s002850200143)

57. Famili I, Palsson BO. 2003 Systemic metabolic reactions are obtained by singular value decomposition of genome-scale stoichiometric matrices. *J. Theor. Biol.* **224**, 87–96. (doi:10.1016/S0022-5193(03)00146-2)

58. Famili I, Palsson BO. 2003 The convex basis of the left null space of the stoichiometric matrix leads to the definition of metabolically meaningful pools. *Biophys. J.* **85**, 16–26. (doi:10.1016/S0006-3495(03)74450-6)

59. Gawthrop PJ. 2000 Physical interpretation of inverse dynamics using bicausal bond graphs. *J. Franklin Inst.* **337**, 743–769. (doi:10.1016/S0016-0032(00)00051-X)

60. Ngwompo R, Scavarda S, Thomasset D. 2001 Physical model-based inversion in control systems design using bond graph representation part 2: applications. *Proc. of the I MECH E Part I J. Syst. Control Eng.* **215**, 105–112. (doi:10.1243/0959651011540897)

61. Marquis-Favre W, Jardin A. 2011 Bond graphs and inverse modeling for mechatronic system design. In *Bond graph modelling of engineering systems* (ed. W Borutzky), pp. 195–226. New York, NY: Springer.
62. Sueur C, Dauphin-Tanguy G. 1989 Structural controllability/observability of linear systems represented by bond graphs. *J. Franklin Inst.* **326**, 869–883. (doi:10.1016/0016-0032(89)90009-4)
63. Reder C. 1988 Metabolic control theory: a structural approach. *J. Theor. Biol.* **135**, 175–201. (doi:10.1016/S0022-5193(88)80073-0)
64. Ingalls BP, Sauro HM. 2003 Sensitivity analysis of stoichiometric networks: an extension of metabolic control analysis to non-steady state trajectories. *J. Theor. Biol.* **222**, 23–36. (doi:10.1016/S0022-5193(03)00011-0)
65. Ingalls BP. 2004 A frequency domain approach to sensitivity analysis of biochemical networks. *J. Phys. Chem. B* **108**, 1143–1152. (doi:10.1021/jp036567u)
66. Sauro HM. 2009 Network dynamics. In *Computational systems biology* (eds R. Ireton, K. Montgomery, R. Bumgarner, R. Samudrala, J. McDermott). Methods in Molecular Biology, vol. 541, pp. 269–309. Totowa, NJ: Humana Press.
67. Ingalls BP. 2013 *Mathematical modelling in systems biology*. Cambridge, MA: MIT Press.
68. Kraeutler M, Soltis A, Saucerman J. 2010 Modeling cardiac beta-adrenergic signaling with normalized-hill differential equations: comparison with a biochemical model. *BMC Syst. Biol.* **4**, 157. (doi:10.1186/1752-0509-4-157)
69. Ryall KA, Holland DO, Delaney KA, Kraeutler MJ, Parker AJ, Saucerman JJ. 2012 Network reconstruction and systems analysis of cardiac myocyte hypertrophy signaling. *J. Biol. Chem.* **287**, 42 259–42 268. (doi:10.1074/jbc.M112.382937)
70. Tran K, Smith NP, Loiselle DS, Crampin EJ. 2009 A thermodynamic model of the cardiac sarcoplasmic/endoplasmic $Ca^{2+}$ (SERCA) pump. *Biophys. J.* **96**, 2029–2042. (doi:10.1016/j.bpj.2008.11.045)
71. Fink M *et al.* 2011 Cardiac cell modelling: observations from the heart of the cardiac physiome project. *Progr. Biophys. Mol. Biol.* **104**, 2–21. (doi:10.1016/j.pbiomolbio.2010.03.002)
72. Lloyd CM, Halstead MDB, Nielsen PF. 2004 CellML: its future, present and past. *Progr. Biophys. Mol. Biol.* **85**, 433–450. (doi:10.1016/j.pbiomolbio.2004.01.004)
73. Hucka M *et al.* 2003 The systems biology markup language (SBML): a medium for representation and exchange of biochemical network models. *Bioinformatics* **19**, 524–531. (doi:10.1093/bioinformatics/btg015)
74. Cooling MT, Hunter P, Crampin EJ. 2008 Modelling biological modularity with CellML. *Syst. Biol. IET* **2**, 73–79. (doi:10.1049/iet-syb:20070020)
75. Frank PM. 1978 *Introduction to system sensitivity theory*. New York, NY: Academic Press.
76. Rosenwasser E, Yusupov R. 2000 *Sensitivity of automatic control systems*. Boca Raton, FL: CRC Press.
77. Heinrich R, Schuster S. 1996 *The regulation of cellular systems*. New York, NY: Chapman & Hall.
78. Karnopp D. 1977 Power and energy in linearized physical systems. *J. Franklin Inst.* **303**, 85–98. (doi:10.1016/0016-0032(77)90078-3)
79. Gawthrop PJ. 2000 Sensitivity bond graphs. *J. Franklin Inst.* **337**, 907–922. (doi:10.1016/S0016-0032(00)00052-1)
80. Gawthrop PJ, Ronco E. 2000 Estimation and control of mechatronic systems using sensitivity bond graphs. *Control Eng. Practice* **8**, 1237–1248. (doi:10.1016/S0967-0661(00)00062-9)
81. Sueur C, Dauphin-Tanguy G. 1997 Controllability indices for structured systems. *Linear Algebra Appl.* **250**, 275–287. (doi:10.1016/0024-3795(95)00598-6)
82. Fotsu Ngwompo R, Scavarda S, Thomasset D. 1996 Inversion of linear time-invariant SISO systems modelled by bond graph. *J. Franklin Inst.* **333**, 157–174. (doi:10.1016/0016-0032(96)00025-7)
83. Ngwompo RF, Gawthrop PJ. 1999 Bond graph based simulation of nonlinear inverse systems using physical performance specifications. *J. Franklin Inst.* **336**, 1225–1247. (doi:10.1016/S0016-0032(99)00032-0)